

IDŐJÁRÁS

*Quarterly Journal of the Hungarian Meteorological Service
Vol. 126, No. 4, October – December, 2022, pp. 457–480*

Investigation of a supercell merger leading to the EF4 tornado in the Czech Republic on June 24, 2021 using radar data and numerical model outputs

**Kornél Komjáti^{1,2,5,*}, Ákos János Varga², Ladislav Méri^{3,4},
Hajnalka Breuer², and Sándor Kun⁵**

¹*Hungarian Meteorological Service
Kítaibel Pál u. 1, Budapest H-1024, Hungary*

²*ELTE Eötvös Loránd University
Institute of Geography and Earth Sciences
Department of Meteorology
Pázmány Péter sétány 1/A, Budapest H-1117, Hungary*

³*Slovak Hydrometeorological Institute
Jeséniova 17, 833 15 Bratislava, Slovakia*

⁴*Department of Astronomy, Physics of the Earth and Meteorology
Comenius University in Bratislava, 842 48 Bratislava, Slovakia*

⁵*Hungarian Association of Stormchasers and Storm Damage Surveyors
Fiastyúk u. 57. 3/3., Budapest H-1139, Hungary*

**Corresponding author E-mail: komjati.k@met.hu*

(Manuscript received in final form January 24, 2022)

Abstract— An unprecedented deadly and destructive EF4 tornado struck the Czech Republic across Břeclav and Hodonín districts on June 24, 2021. On this day, several supercells developed in Central Europe, however, in Austria and the Czech Republic region only one cell produced a tornado. For this reason, in addition to the macrosynoptic setup, it is also worth exploring the small-scale cell interactions that can lead to the formation of a devastating EF4 tornado. We use ECMWF analysis and forecast fields, sounding profiles, and radar measurements to examine the synoptic weather situation and convective processes. Moreover, to investigate the evolution and structure of convection, two Weather Research and Forecasting (WRF) model simulations were carried out at 1.5 km grid spacing with one-moment and two-moment microphysical parameterizations. WRF captures the overall spatial distribution and supercellular nature of thunderstorms, although discrepancies exist in the magnitude and spatial location of individual cells. The low-reflectivity region accompanying the thunderstorms is better represented by the one-moment microphysics scheme.

Key-words: supercell, tornado, cell merger, convection, thunderstorm, WRF model, numerical simulation

1. Introduction

On June 24, 2021, an unusually strong tornado formed in southeast Czechia, resulting in at least 6 deaths, and injuring more than 200 people. Based on the available information and the caused damage, the European Severe Storm Laboratory (ESSL) rated the tornado as category 4 on the Enhanced Fujita Scale (EF4). The specialty of the case was that before the tornadogenesis, the tornado-producing mother supercell merged with another supercell, similarly to the historic May 22, 2011 Joplin (USA, Missouri) tornado (*Van Leer, 2013, Knupp et al., 2014*).

The importance of the storm merger in tornadogenesis has been discussed in several papers (*Bluestein and Weisman, 2000; Lee et al., 2006, Wurman et al., 2007, Van Leer, 2013*). The definition of cell merging is generally based on radar observations and describes the union of two, initially independent radar echoes (*Westcott and Kennedy 1989; Lee et al., 2006*), or the merging of the updraft region (*Wescott, 1994; Bluestein and Weisman, 2000; Hastings and Richardson, 2016*). The success of a merger strongly depends on the angle at which the cells interact with each other, namely if the merger occurs in the inflow region of the mother cell, the downdraft might cut off the main updraft of the mother cell, destroying the storm (*Jaret et al., 2008*). In addition, the strength of the outflow and the distance between the cells are also important (*Hastings and Richardson, 2016*). A typical sign of an effective merger is the reflectivity cloud bridge between the cells (*Simpson et al., 1980*), created by the downdraft outflow boundaries.

In recent years, much attention has been paid to studying multiple gust front convergence zones and their role in tornadogenesis (*Marquis et al., 2008; Beck and Weiss, 2013; Orf et al., 2017; Betten et al., 2018; Schueth et al., 2021*). There are many questions about the dynamic processes that might be relevant in the production of the secondary rear flank gust front and its adverse or advantageous effect on near-surface stretching. Although, in several cases, it is seen that the secondary boundary on the surface inside of the rear flank downdraft (RFD) region might contribute to the low-level mesocyclone intensification through the multiple convergent zones and the horizontal wind-shift generated vorticity. However, a secondary rear flank gust front may also appear not only inside a supercell, but with a connection of different downdraft regions as well during a cell-merger process (*Van Leer, 2013*), or cell interaction with a remnant outflow boundary (*Markowski et al., 1998*).

The Weather Research and Forecasting (WRF) model is an increasingly popular tool for the numerical simulation of weather-related phenomena in both operational and academic applications (*Powers et al., 2017*). It has been used extensively to model tornado-producing supercell thunderstorms (e.g., *Miglietta et al., 2017; Scheffknecht et al., 2017; Pigluj et al., 2019; Spiridonov et al., 2021*). Numerical studies of supercells require convection-allowing (< 4 km) grid sizes,

where the role of the microphysical parameterization becomes crucial (*Johnson et al.*, 2016). It has been argued that two-moment schemes that also predict the number concentration of hydrometeor species can improve on the results of one-moment parameterizations when modeling convection-related processes (e.g., *Dawson et al.*, 2010; *Jung et al.*, 2012).

In the current study, we aim to examine the effect of environmental conditions, particularly the potential impact of the cell-merger on the tornadogenesis with ECMWF (European Centre for Medium-Range Weather Forecasts) IFS (Integrated Forecasting System) model products, atmospheric soundings requested from the Hungarian Meteorological Service, and real-time radial base velocity measurements and CAPPI (Constant Altitude Plan Position Indicator) planes from the Slovak Hydrometeorological Institute. Additionally, we utilize two WRF simulations with one- and two-moment microphysics schemes to study the evolution and structure of convection on the day of tornadic supercell occurrence at the Slovakian-Czech border. The aim is to investigate the capability of WRF to capture the spatiotemporal pattern and supercellular nature of thunderstorms.

2. Synoptic and mesoscale overview and storm formation

2.1. Forecasted synoptic and mesoscale conditions

In the afternoon of June 24, 2021, a strong, extended frontal boundary was located in Central Europe, which separated the Atlantic air mass from the unstable, moist air of southern and eastern Europe (*Fig. 1, top*). As the frontal zone crossed the Alps, a warm frontal wave formed on it, which caused a surface low on the lee side of the Alps. Above the warm frontal stage of the boundary in the upper levels, a short-wave trough spread northeast (*Fig. 1, bottom*) with a mid-level jet, which extended from the Mediterranean Sea to Poland (*Fig. 2, top*). In the lower levels, alongside the boundary, a strengthening low-level jet was forecasted for 18:00 UTC, which started to spread up from the Mediterranean Sea through the Czech-Slovakian border to the Baltic states (*Fig. 2, bottom*).

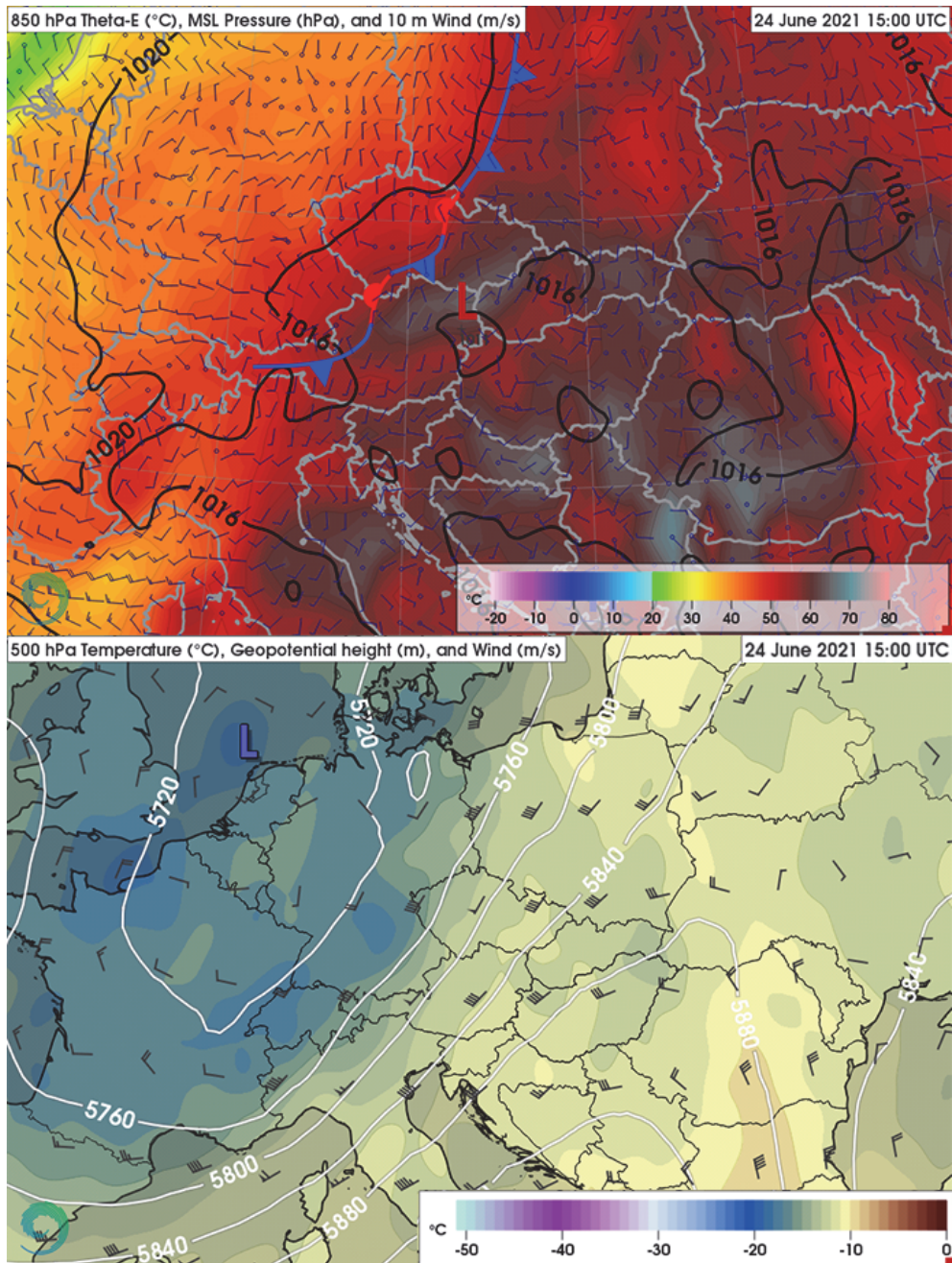


Fig. 1. ECMWF June 24, 2021 15:00 UTC forecast of 850 hPa equivalent potential temperature (shaded), surface pressure (solid black lines), fronts, and 10 m wind (blue barbs) (top). ECMWF June 24, 2021 15:00 UTC forecast of 500 hPa temperature (shaded), geopotential height (solid white lines), and wind (black barbs) (bottom).

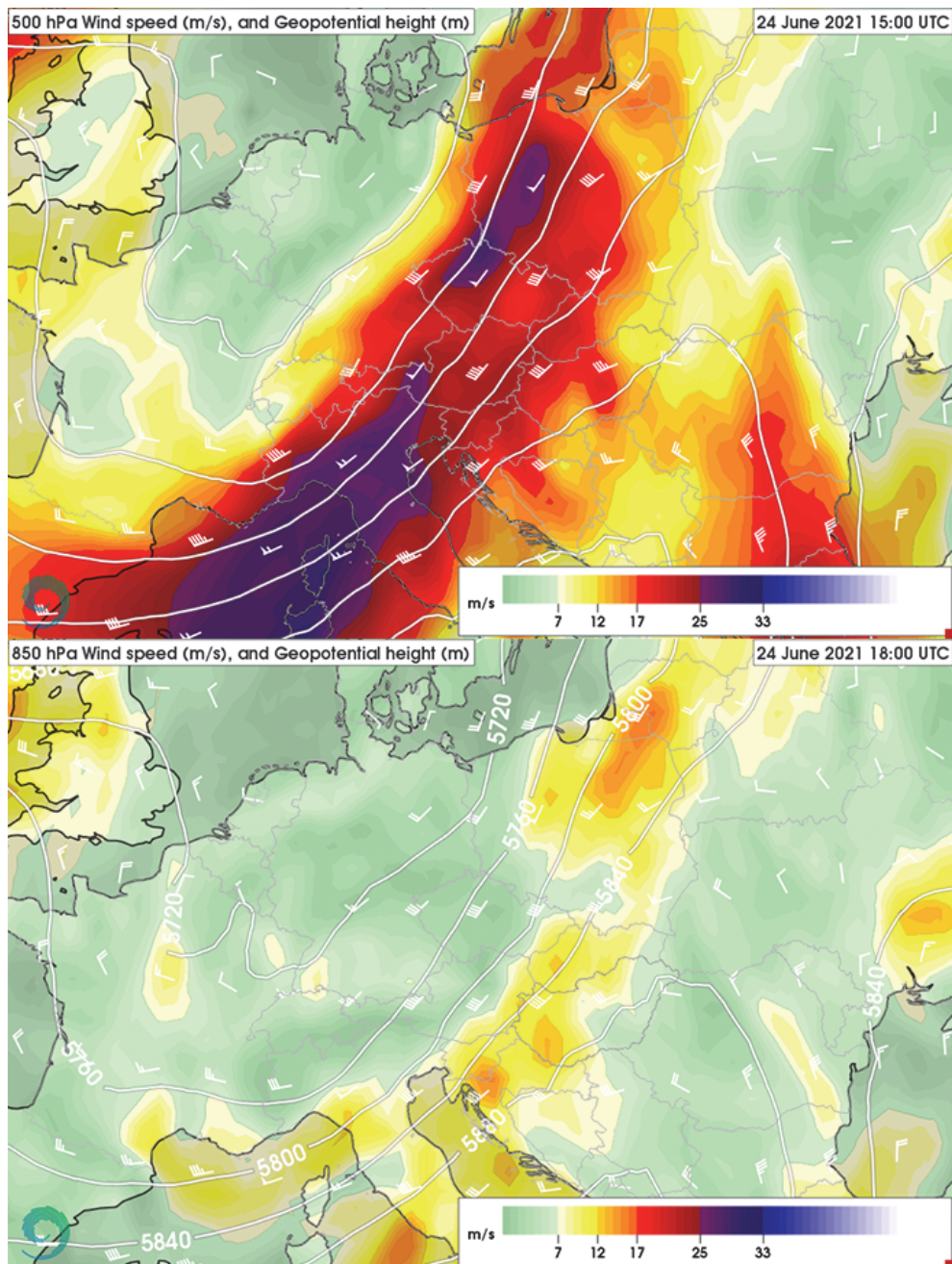


Fig. 2. ECMWF June 24, 2021 15:00 UTC forecast of 500 hPa wind speed (shaded), geopotential height (solid white lines), and wind (white barbs) (top). ECMWF June 24, 2021 18:00 UTC forecast of 850 hPa wind speed (shaded), geopotential height (solid white lines), and wind (white barbs) (bottom).

The convective initiation started in a very unstable and moist environment as predicted by the ECMWF IFS model (with 60–62 °C equivalent potential temperature and 2500–3000 J kg⁻¹ CAPE (convective available potential energy) maxima) in Central Austria. In the warm sector, a near-surface confluent flow

(caused by the above-mentioned developing surface low and the orography) triggered the deep convective activity. Besides the convergent zones, the cyclonic flow resulted in northeastern wind components at the backside of the pressure minima at 15:00 UTC, which induced a strong storm-relative inflow and a notable curvature in the wind profile in the lowest 1000 m for the developing thunderstorms (*Fig. 3*). Thus, the developing surface low and the strengthening mid-level flow, together with the increasingly curved hodograph and the high environmental bulk shear ($25\text{--}30\text{ ms}^{-1}$ for the 0–6 km layer), supplemented by the unstable, humid air mass resulted in especially favorable conditions for supercells. The storm-relative helicity for the right-moving cells (SREH-R) in the 0–3 vertical layer, and the supercell composite parameter (SCP) also showed that the conditions were ideal for intense supercells (*Fig. 4*). These favorable parameters particularly aligned with each other at around 15:00 UTC in the forecast over the central and western parts of the Lower Austria region. However, increased values of tornadic parameters (significant tornado parameter (STP), 0–1 km SREH-R, and the 0–1 km bulk shear) were predicted only at around 18:00 UTC (*Fig. 5*), when the low-level jet started to strengthen.

ECMWF WIEN Hodograph Thursday 24 Jun 2021 15:00 (+3h) :-----

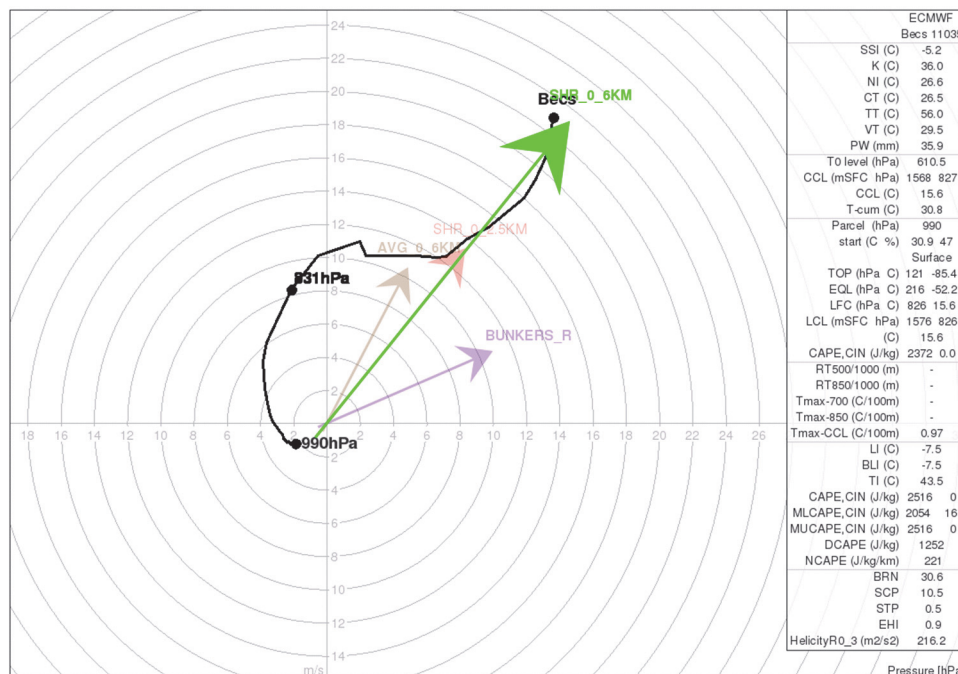


Fig. 3. ECMWF June 24, 2021 15:00 UTC forecast of hodograph over Wien-Hohe Warte. Wind shear profile between 0 and 500 hPa (solid black line), 0–6 km bulk shear vector (green arrow), 0–2.5 km bulk shear vector (red arrow), 0–6 km bulk mean wind vector (brown arrow), and the Bunkers storm motion vector for right-moving supercells (purple

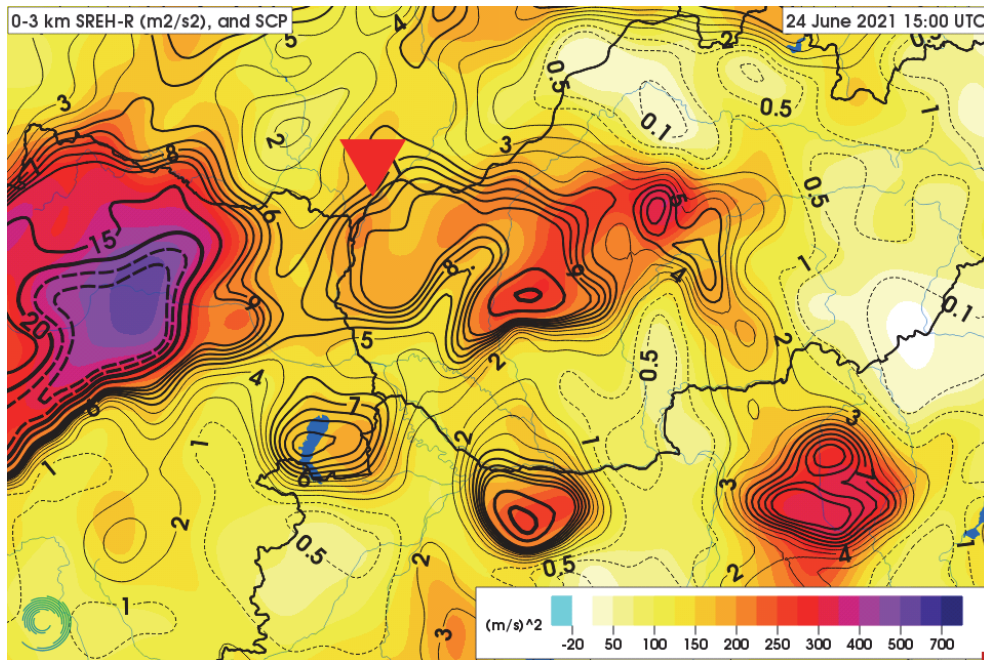


Fig. 4. ECMWF June 24, 2021 15:00 UTC forecast of 0–3 km storm relative helicity for right-moving supercells (SREH-R; shaded), and the supercell composite parameter (SCP; solid and dashed black lines). The red triangle depicts the observed position of the tornado.

2.2. Storm formation and evolution

The 12:00 UTC sounding over Wien – Hohe Warte revealed that the forecasted unstable environment mentioned above was indeed accomplished: 2228 J kg⁻¹ CAPE, -3.2 °C SSI, 54.7 TT (*Fig. 6, top*). The soundings showed a classical Great Plains Type setup (*Gordon and Albert, 2000*) with a mid-level dry air bulge, some capping at 850 hPa, and relatively high, ≈19°C dew point temperature with a steep profile in the lowest 100 hPa. The Prostějov (Czech Republic) soundings showed a more unstable environment but slightly drier mid-level conditions (*Fig. 6, bottom*).

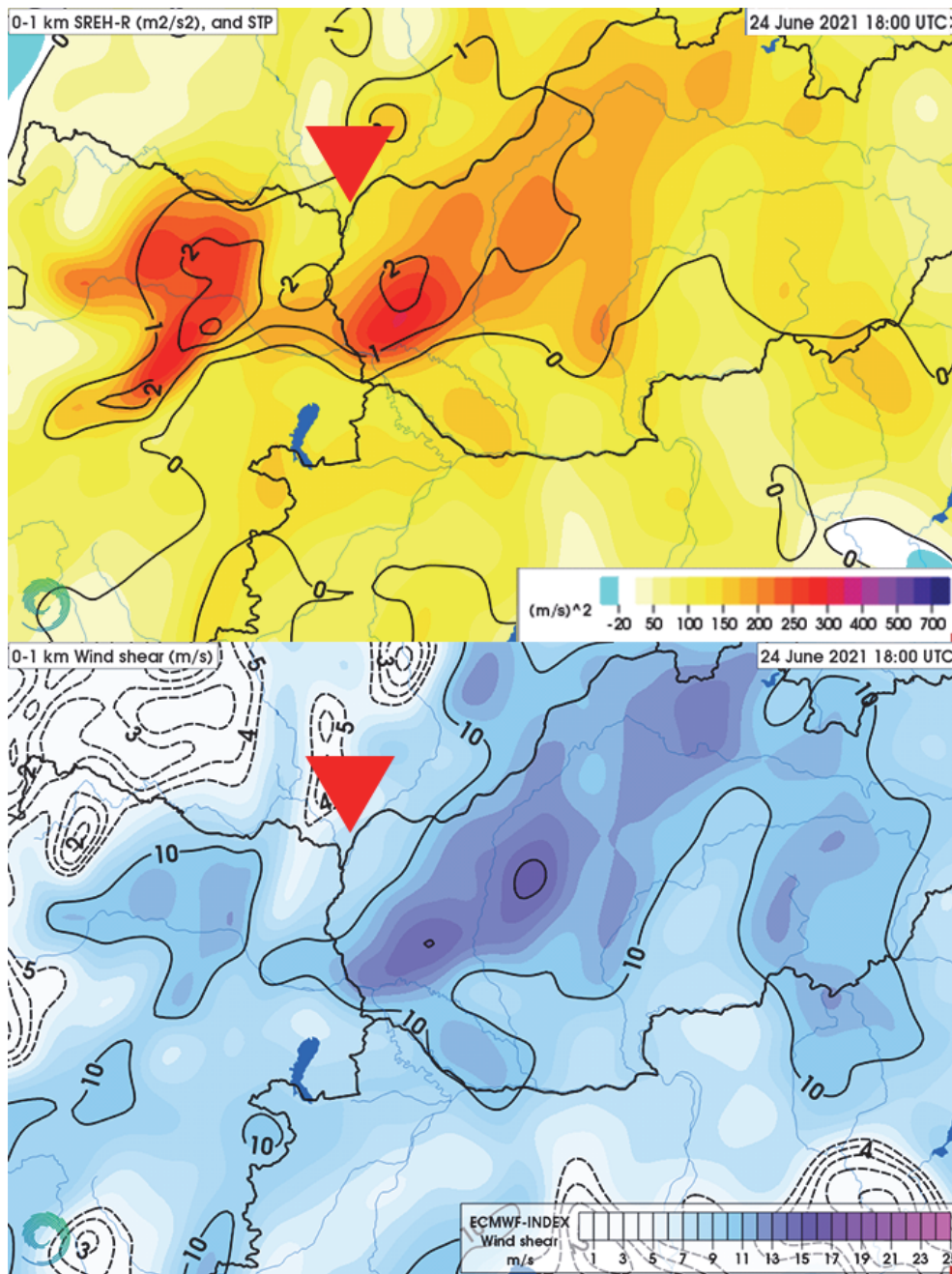


Fig. 5. ECMWF June 24, 2021 18:00 UTC forecast of 0–1 km storm-relative helicity for right-moving supercells (SREH-R; shaded), and the significant tornado parameter (STP; solid and dashed black line) (top). ECMWF June 24, 2021 18:00 UTC forecast of 0–1 km bulk shear (shaded, and solid black lines), and the observed position of the tornado (red triangle) (bottom).

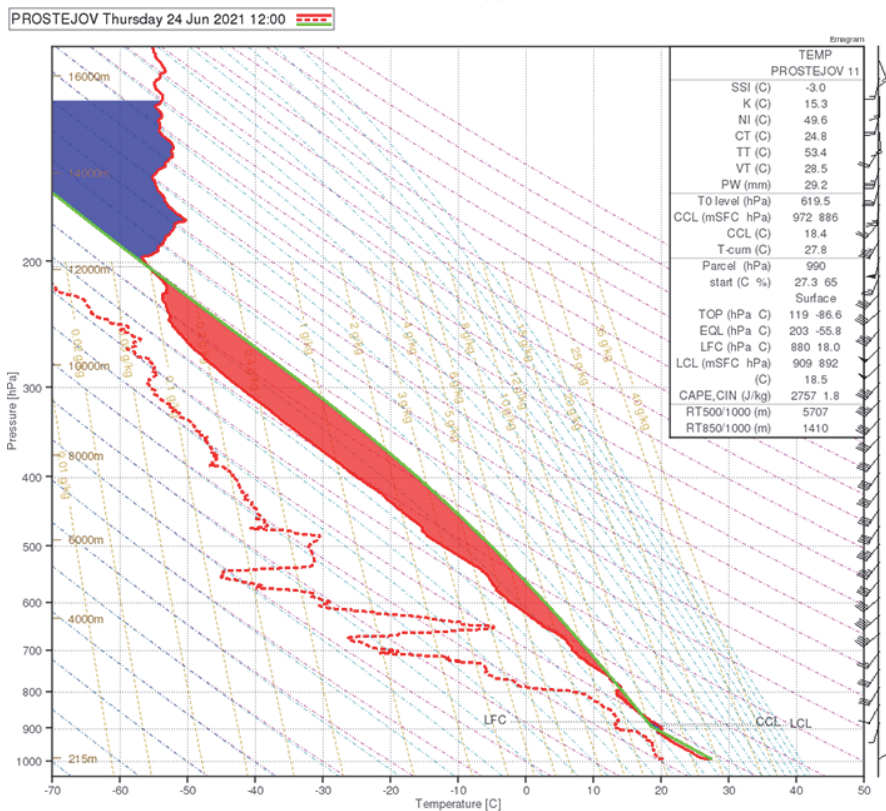
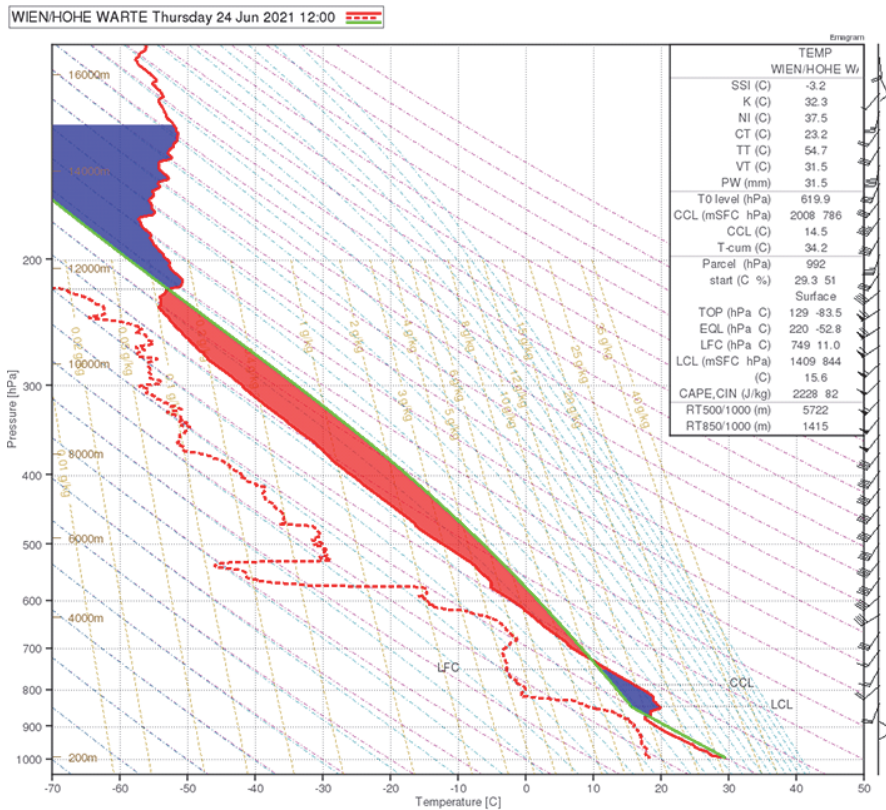


Fig. 6. Upper air data at the initiation time (June 24, 2021 12:00 UTC) in Wien – Austria (top), and Prostejov – Czech Republic (bottom). The stable (unstable) area of the sounding is shaded by blue (red).

The first thunderstorm of the day initiated at 12:00 UTC over Austria, triggered by the orographic lifting effect, and started to move to the northeast. At 13:05 UTC, a supercell (C1) started to form at the boundary of the left member of the splitting supercell at the border of Styria and Lower Austria regions (not shown). After the first thunderstorms, at around 15:00 UTC gradually more and more cells initiated over the central and the western part of Lower Austria.

Over these areas, as shown in *Fig. 4.*, the forecasted SCP and SREH-R values guaranteed exceptionally suitable conditions for intensive supercells, and as a result, a cell (C2) appeared at 14:30 UTC over Krems an der Donau. The C2 thunderstorm became a strong supercell which was indicated by the well-defined hook echo as well at 15:30 UTC (*Fig. 7*).

During the development of the C2 supercell, the C1 supercell started to split under favorable conditions and the left-mover member (C1/L) showed up on radar at 15:20 UTC. The deviantly moving C1/L cell gradually approached the C2 cell toward its RFD (rear flank downdraft) region. The merger of C1/L and C2 occurred at a nearly perfect angle, thus the downdraft region of C1/L penetrated the RFD of C2. This process might have created an external secondary gust front that provided a new source of surface convergence for the main updraft (*Fig. 8*). This transport may have contributed to the intensification of the low-level mesocyclogenesis, resulting in an even more definite right turn in C2's movement.

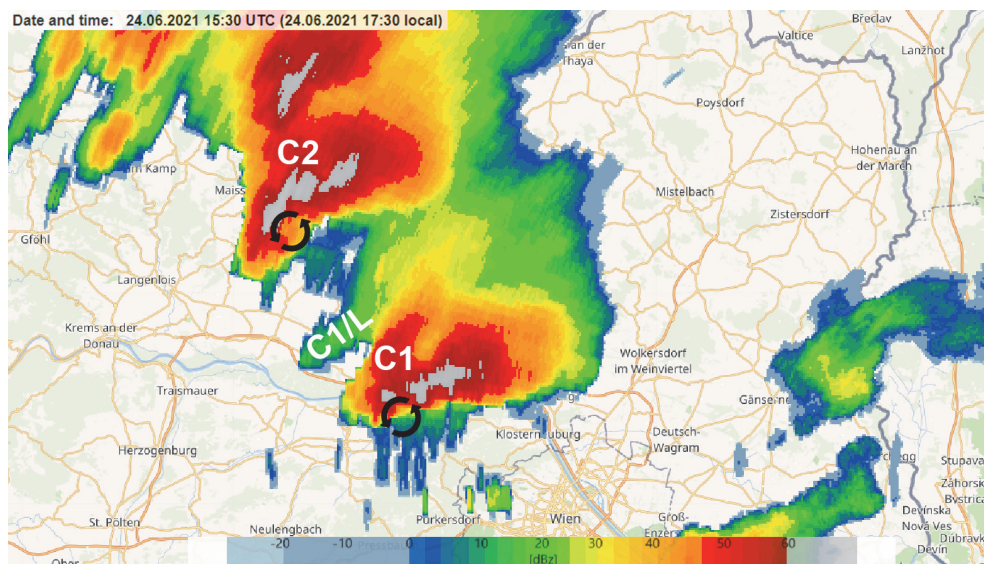


Fig. 7. 2 km CAPPI radar reflectivity (dBz) plane valid for June 24, 2021 15:30 UTC. The black rotating arrows represent the low-level mesocyclones of C1 and C2 supercells. C1/L is the left-mover member of the splitting C1 supercell.

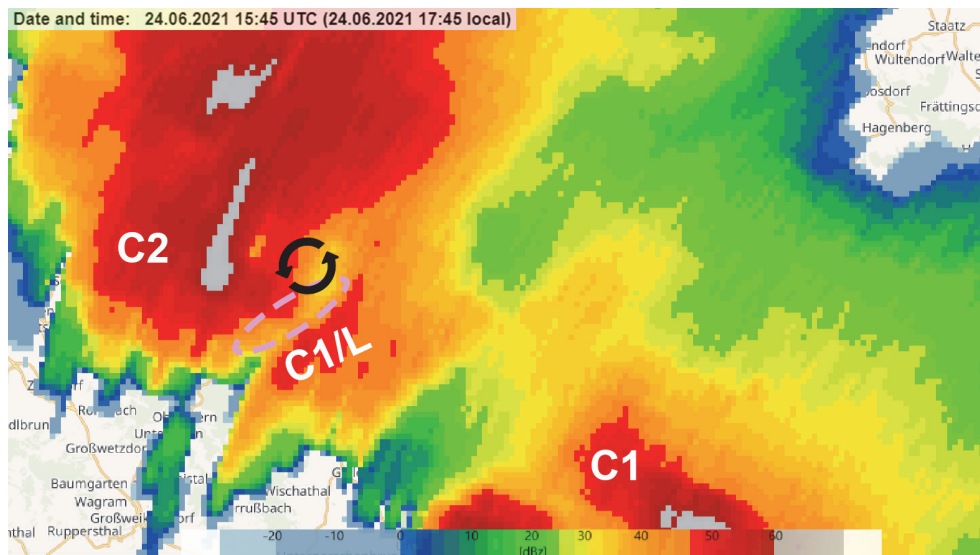


Fig. 8. 2 km CAPPI radar reflectivity (dBz) plane valid for June 24, 2021 15:45 UTC. The black rotating arrows represent the low-level mesocyclone of the C2 supercell. C1/L is the left-mover member of the splitting C1 supercell. The purple dashed ellipse depicts the effective merging area.

The rapid evolution of C2's mesocyclone indicated an interaction with the surrounding C1 supercell. The faster moving C2 started to approach C1 progressively, and at 16:00 UTC a reflectivity bridge cell appeared between the merging cells generated by the downdraft regions (*Fig. 9, top*). At 16:10 UTC, C2's more intensive and faster RFD gust front spread out and started to connect with the C1's RFD (*Fig. 9, bottom*). In a similar way to the interaction between C1/L and C2, the RFD regions combined and presumably resulted in an external secondary gust front in C1's RFD near-surface flow field. The merger process was completed at around 16:20 UTC. Based on the radar images, the cell interaction was especially beneficial for the supercell, and the regenerating low-level mesocyclone became very intense in a short time. Approximately 20 minutes after the merging, at 16:50 UTC¹, the C1 supercell reached the border of the Czech Republic with a noticeable hook echo (*Fig. 10, top*) and possibly a TVS (Tornado Vortex Signature) inside the mesocyclone. The neighboring pixels showed -30 ms^{-1} inbound and $+30 \text{ ms}^{-1}$ outbound values on the base velocity field (*Fig. 10, bottom*).

¹ At this time in addition to the effect of the cell-merger, the strengthening low-level jet probably also aided the intensification of the supercell.

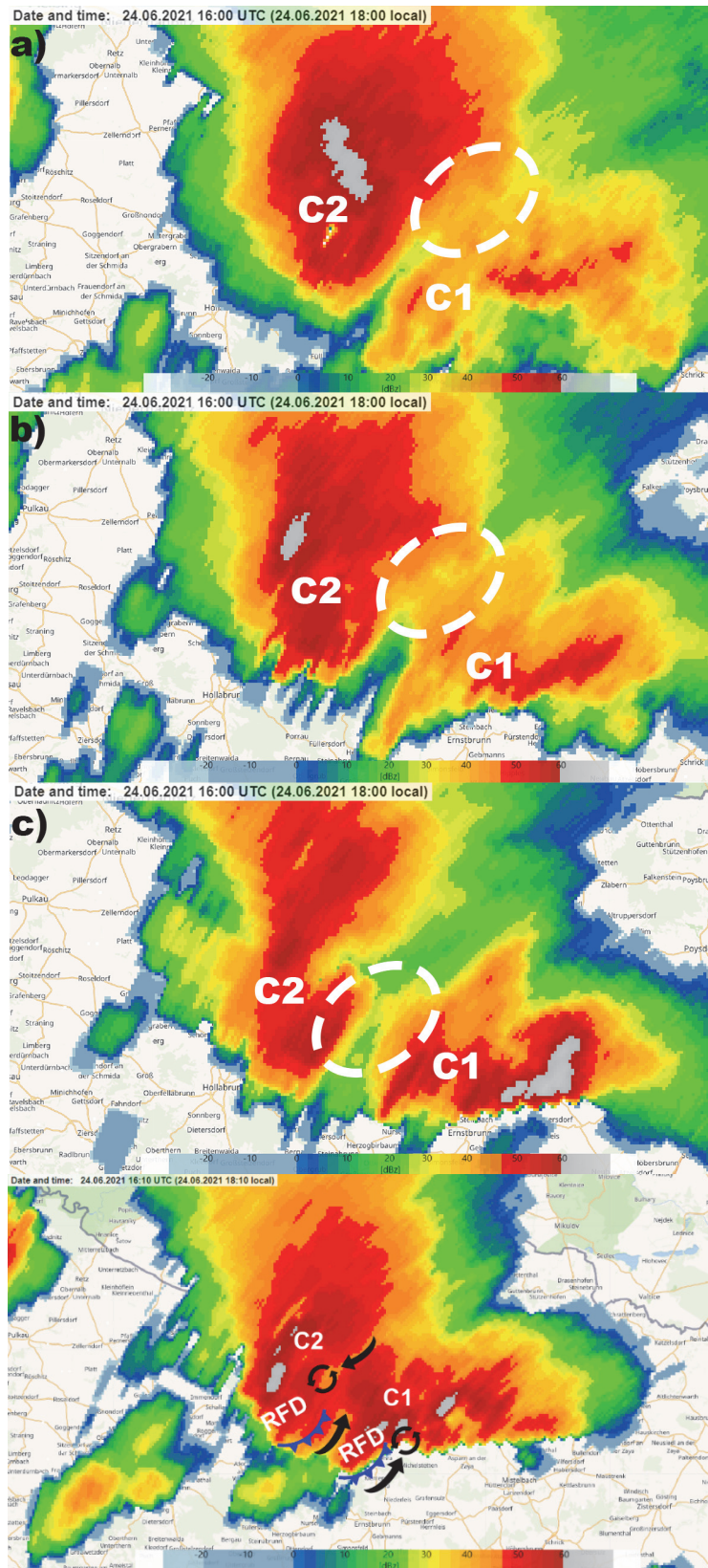


Fig. 9. 2 km (a), 4 km (b), and 6 km (c) CAPPI radar reflectivity (dBZ) plane valid for June 24, 2021 16:00 UTC. The dashed white ellipses depict the reflectivity bridge between the merging storms (top). 2 km CAPPI radar reflectivity (dBZ) plane is valid for 24 June 2021 16:00 UTC (bottom). The black rotating arrows represent the low-level mesocyclone of supercells C1 and C2. The black curved arrows show the inflow notches, and the blue fronts represent the rear inflow downdraft (RFD) gust fronts.

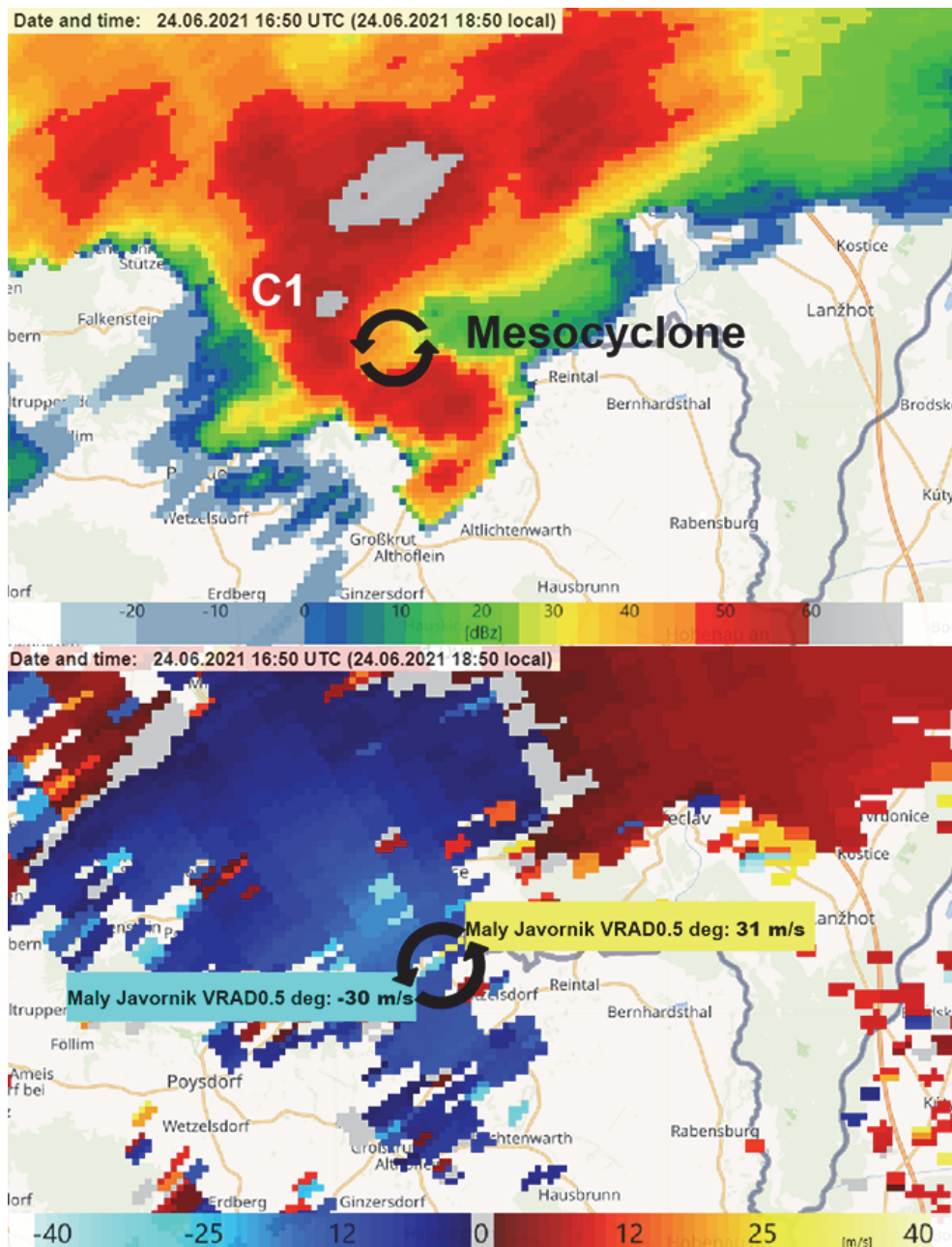


Fig. 10. 2 km CAPPI radar reflectivity (dBz) plane valid for 24 June 2021 16:50 UTC (top). Possible tornado vortex signature can be seen on the 0.5 degrees radial base velocity measurement (ms^{-1}) valid for June 24, 2021 16:50 UTC (bottom). The black rotating arrows represent the low-level mesocyclone, the bluish shades represent the inbound motions, and the reddish and yellow shades depict the outbound movement.

At 17:05 UTC in the Czech Republic over Břeclav, a tornado-like vortex appeared on the 2 km CAPPI with a donut-shaped signature (Fig. 11), which refers to a low-reflectivity eye with an intensive updraft region (Wood *et al.*, 2009). This donut hole signature was continuously present when the first

touchdown was observed in Hrušky at 17:20 UTC (*Fig. 12*). After the first observation, the tornado continued its path along the Slovakian and Czech border causing serious damages in Moravská Nová Ves, Lužice, and Hodonín towns, causing at least 6 deaths, and injuring more than 200 people. According to the reports, the tornado left Hodonín and dissipated at around 17:45 UTC.

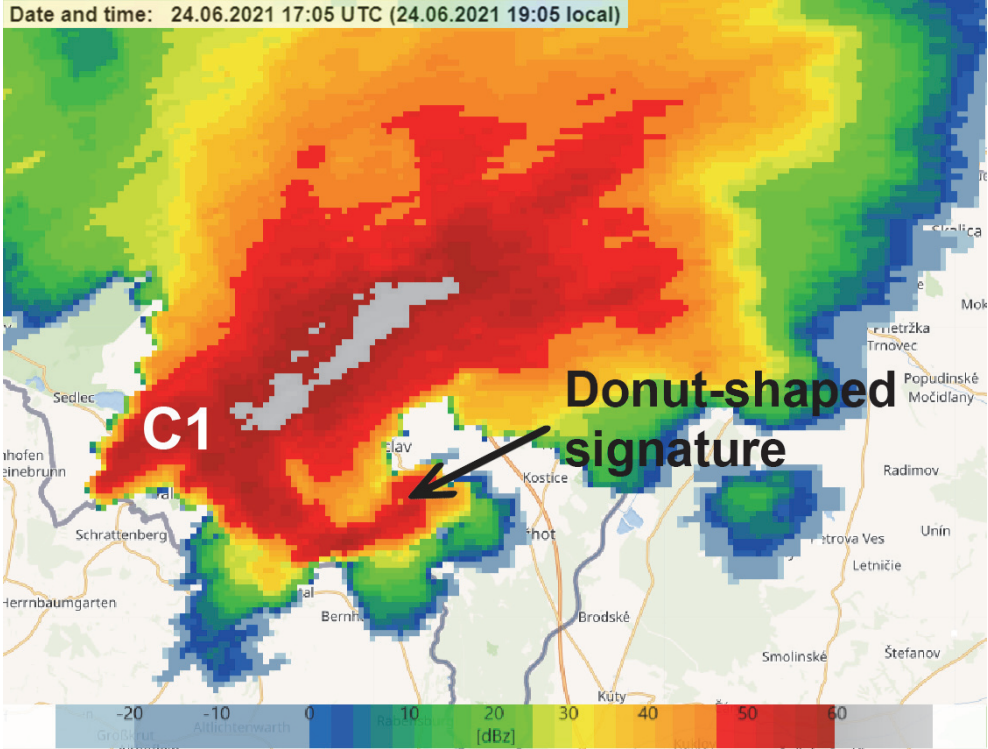


Fig. 11. Potential tornado-like vortex on the 2 km CAPPI radar reflectivity (dBz) plane valid for June 24, 2021 17:05 UTC.

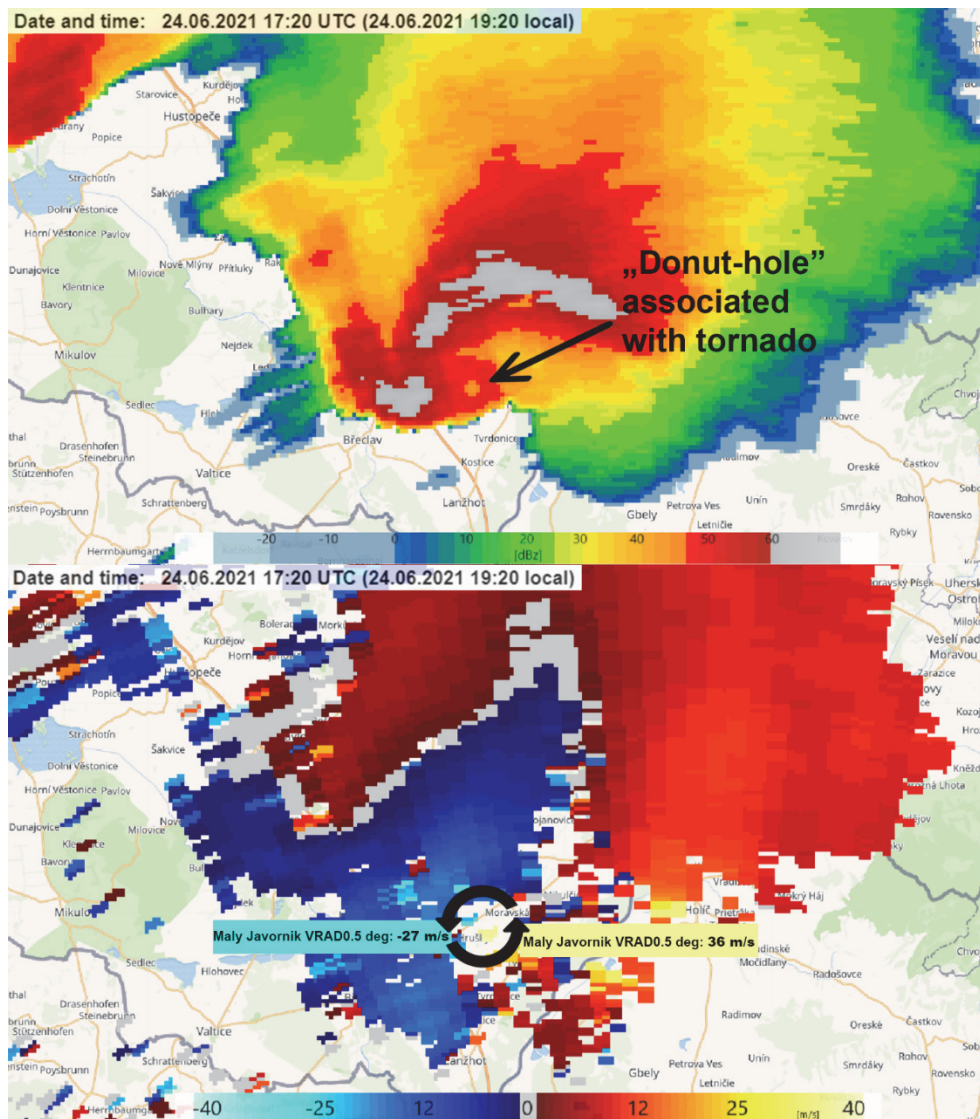


Fig. 12. Donut-shaped radar signature associated with a tornado on the 2 km CAPPI radar reflectivity (dBz) plane valid for June 24, 2021 17:20 UTC (top). Possible tornado vortex signature can be seen on the 0.5 degrees radial base velocity measurement (ms^{-1}) valid for June 24, 2021 17:20 UTC (bottom). The black rotating arrows represent the low-level mesocyclone, the bluish shades represent the inbound motions, and the reddish and yellow shades depict the outbound movement.

3. WRF simulations

3.1. Model settings

The non-hydrostatic mesoscale Advanced Research WRF (ARW) version 4.2 (Skamarock et al., 2019) was applied to investigate the spatiotemporal evolution of convective processes and cell structure. The WRF model was set up on a Lambert conformal projection comprising 720 and 666 grid points in the west-east and south-north directions, respectively, with a horizontal grid spacing of

1.5 km and 61 hybrid σ -p levels in the vertical. The domain focuses on the Central European region. The initial and boundary conditions were derived from 6-hourly analysis fields of the operative IFS model (Cycle 47r2) by ECMWF. The integration period begins at 00:00 UTC on June 24, 2021 and covers 24 hours.

Two numerical experiments were carried out that only differ in the complexity of the microphysical scheme used. One WRF run utilizes the parameterization of *Thompson et al.* (2008), which is two-moment for rain and ice particles, but single-moment for cloud water, snow, and graupel. The other simulation makes use of the *Morrison et al.* (2009) scheme, which is additionally two-moment for cloud water, snow, and graupel, thus representing a more advanced class of microphysics parameterizations. Other physical processes are represented identically in the two simulations: the radiative transfer by the RRTMG scheme (Rapid Radiative Transfer Model for General Circulation Models; *Iacono et al.*, 2008), the land-surface interactions by the Noah-MP land-surface model (*Niu et al.*, 2011), the planetary boundary layer and surface layer exchange processes by the Yonsei University nonlocal closure (*Hong et al.*, 2006) together with the MM5 model's Monin-Obukhov scheme (*Jiménez et al.*, 2012). The deep convection parameterization is turned off in both experiments.

3.2. Simulation results

The WRF-simulated convective cell at the Slovakian-Czech border at the time of the tornado occurrence (at around 17:20 UTC) is considerably weaker than its observed counterpart, regardless of the microphysical parameterization used (*Fig. 13*). In addition, the cell is misplaced to the east, especially in the Morrison run. Although the WRF configuration utilized in this study did not capture the magnitude of the analyzed tornadic supercell in terms of the simulated reflectivity and missed the preceding storm merger, the overall mesoscale spatial pattern is in good agreement with radar observations (*Fig. 14*).

Comparing the two microphysical parameterizations, the Thompson scheme (*Fig. 13, top*) produces smaller and more isolated high-reflectivity regions and larger stratiform precipitation areas than the Morrison scheme (*Fig. 13, bottom*). An extensive region of relatively low (20–30 dBZ) reflectivity can be observed on radar imagery as well (*Fig. 14*), suggesting the suitability of the Thompson scheme to better capture the widespread, moderate precipitation accompanying the convective cells.

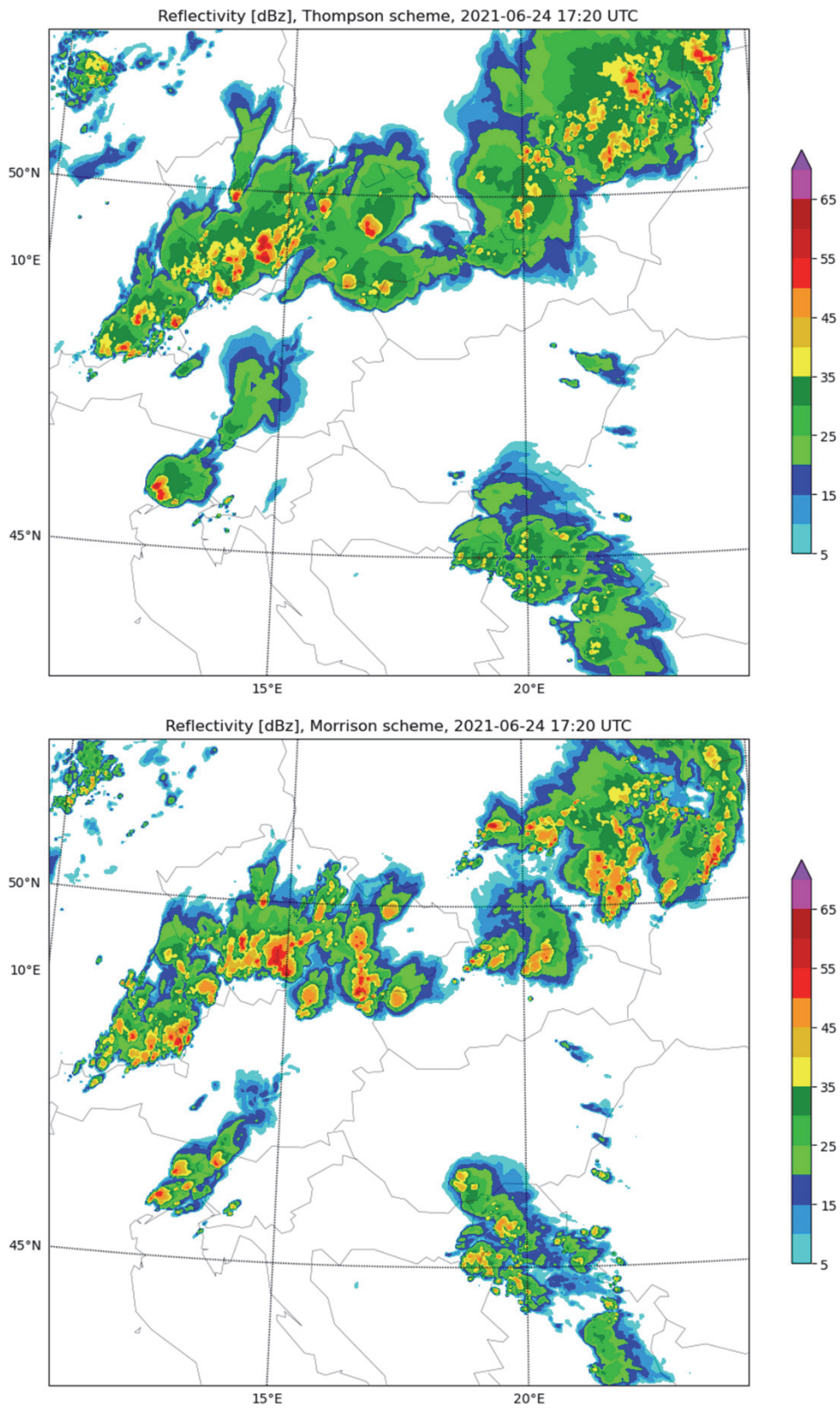


Fig. 13. WRF-simulated composite radar reflectivity valid for June 24, 2021 17:20 UTC, using the Thompson (top) and Morrison (bottom) microphysics parameterization schemes.

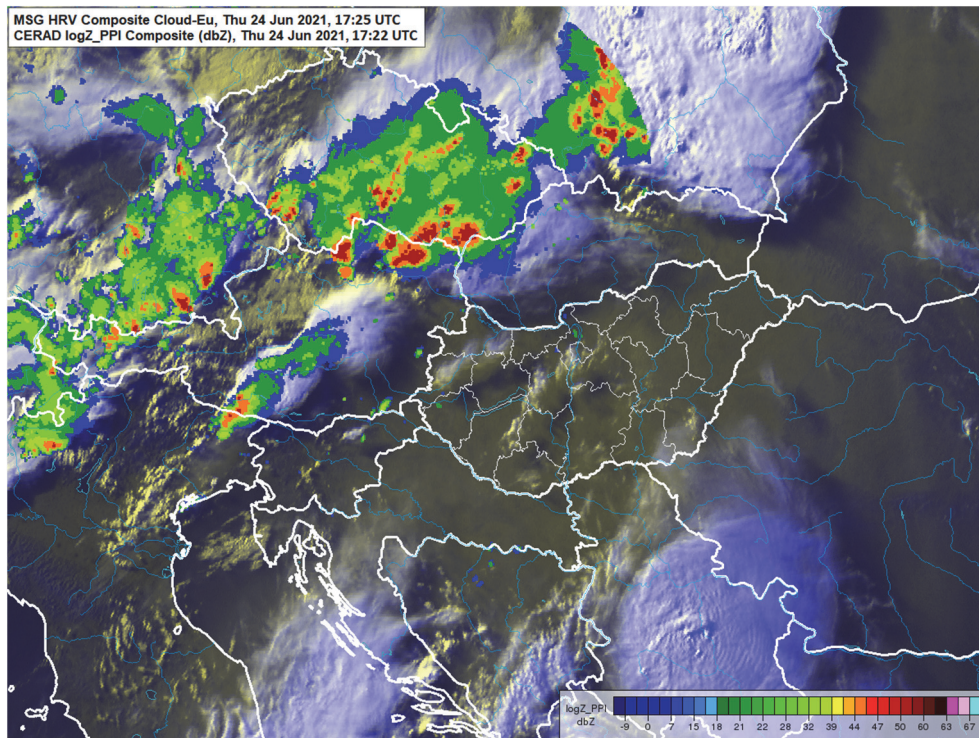


Fig. 14. Supercells over the Central European region: column maximum reflectivity (dBz) of the Central European Radar Network (CERAD), valid for June 24, 2021 17:22 UTC, and the Meteosat Second Generation (MSG) satellite High Resolution Visible (HRV) channel image, valid for 24 June, 2021 17:25 UTC.

In summary, despite requiring more than twice as much computational time, the full two-moment Morrison scheme does not remarkably improve the spatial pattern of simulated radar reflectivity compared to the Thompson parameterization in this specific case. Moreover, the Thompson scheme is used for operational weather prediction purposes even in leading American institutions such as the National Oceanic and Atmospheric Administration (*Benjamin et al.*, 2016). Therefore, results from the Thompson scheme will be presented in the upcoming discussion about storm structure.

Evidence of supercellular convection will be inferred from an arbitrarily selected storm present on the model-derived composite reflectivity field at 16:30 UTC, June 24, 2021 (*Fig. 15*).

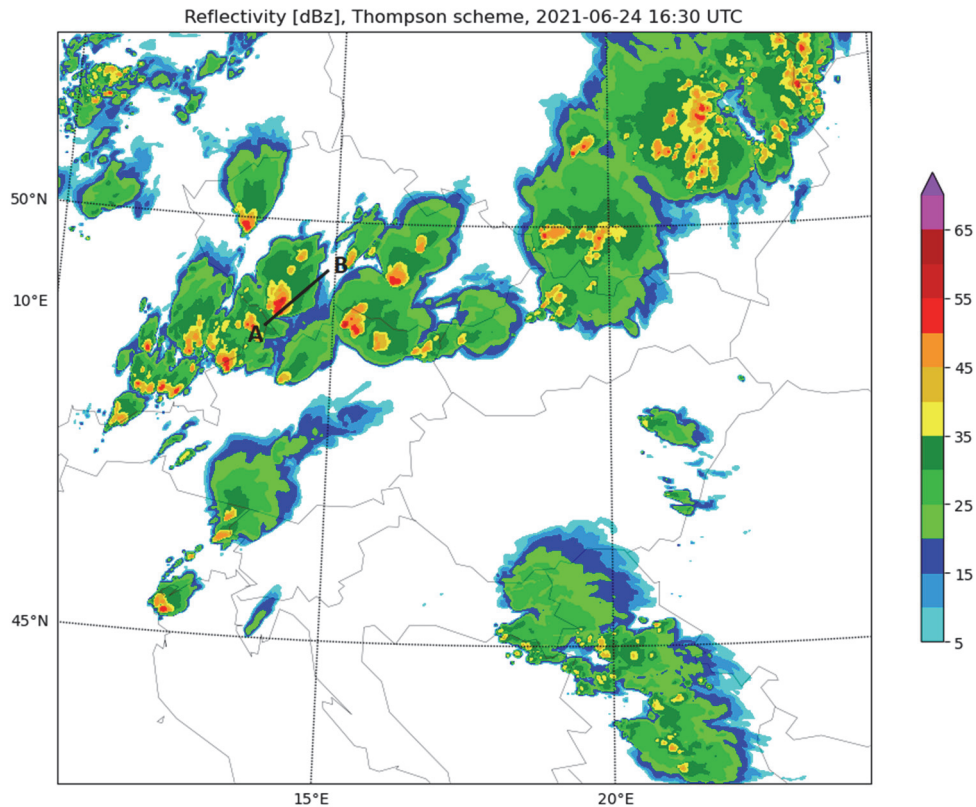


Fig. 15. WRF-simulated composite radar reflectivity valid for June 24, 2021 16:30 UTC, using the Thompson microphysics parameterization. The black line indicates the location of the vertical cross-sections presented in *Fig. 16* and *Fig. 17*.

The vertical cross-sections of reflectivity and vertical velocity (*Fig. 16*) clearly show a typical supercell structure with a bounded weak echo region (BWER) corresponding to the updraft axis. The maximum value of reflectivity and vertical velocity exceeds 55 dBZ and 35 ms^{-1} , respectively. These values, however, refer to this particular cross-section plane and might be higher for the entirety of the convective cell.

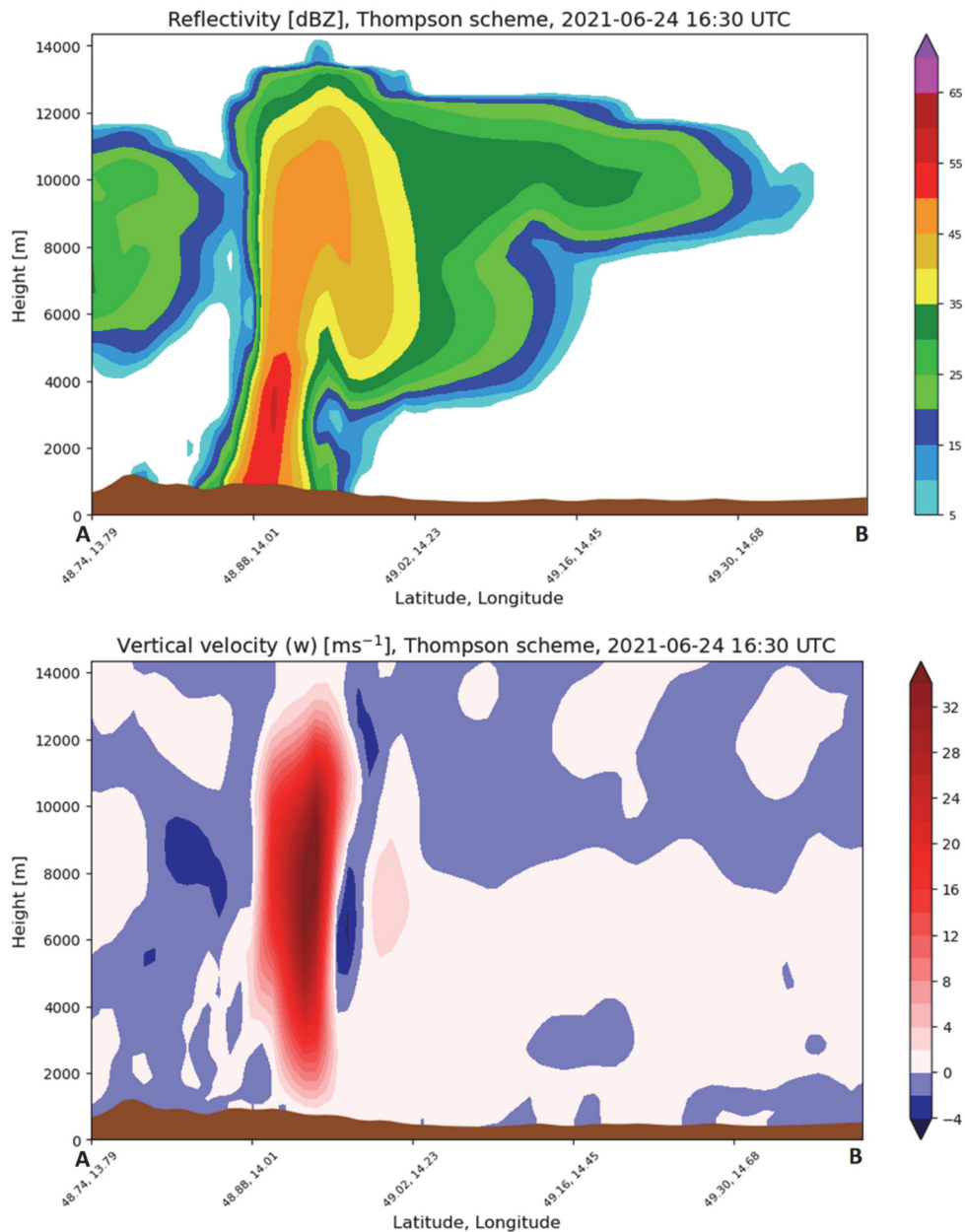


Fig. 16. Vertical cross-section of WRF-simulated radar reflectivity (top) and vertical velocity (bottom) valid for June 24, 2021 16:30 UTC, using the Thompson microphysics parameterization. The location of the vertical cross-sections is indicated by the black line in *Fig. 15*.

The absolute vorticity cross-section implies a rotating updraft with a cyclonic (counter-clockwise) vorticity maximum of $\approx 0.015 \text{ s}^{-1}$ (*Fig. 17*). This is indicative of a mesocyclone, which is a characteristic feature of supercell thunderstorms. The highest values of absolute vorticity can be found at a height of $\approx 6 \text{ km}$, just below the updraft velocity maxima.

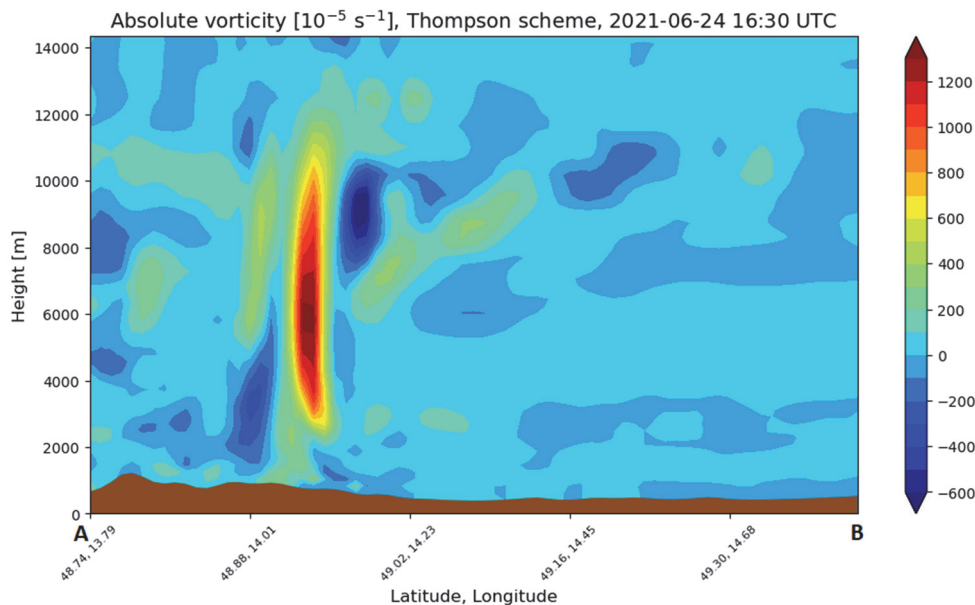


Fig. 17. Vertical cross-section of WRF-simulated absolute vorticity valid for June 24, 2021 16:30 UTC, using the Thompson microphysics parameterization. The location of the vertical cross-section is indicated by the black line in *Fig. 15*.

4. Concluding remarks

Based on the available data in this study, it can be stated, that the suitable environment forecasted by the ECMWF IFS model was approximately realized and aided the development of strong, long-lived supercells. With the strengthening of the low-level jet and deepening of the surface low, the low-level wind shear profile became more favorable for the near-surface vortices. However, only one supercell (marked C1) produced a tornado, namely a destructive EF4 one. Thus, additional effects may have contributed to this local, devastating phenomenon. The most likely contributing factor may have been the cell merger. Based on the radial wind measurements and CAPPI planes from the Radar Malý Javorník (SHMU), two, initially separated right-mover supercells (C1 and C2) merged between 16:00 and 16:20 UTC in Lower Austria resulting in a much stronger supercell structure with an impressive hook echo in a short time. The more intensive and larger C2 cell caught up with the smaller C1 supercell. The faster moving C2 RFD gust front penetrated to the C1 RFD and created an external secondary gust front that may have contributed to the vorticity transport towards the C1 mesocyclone through the emerging secondary surface convergent zone in the RFD. However, the description of the external secondary gust front on the tornadogenesis in this paper is only theoretical, there were no adequate measurements available to justify the process.

Numerical experiments were carried out with the WRF model to study the evolution and structure of convective phenomena on the day of the supercell outbreak at the Slovakian-Czech border. The overall pattern of simulated radar reflectivity is in accordance with radar observations, although the magnitude of the tornadic supercell in focus is considerably weaker in the model. The storm merger was also missed by the simulations. Nevertheless, based on vertical cross-sections of radar reflectivity, vertical velocity, and absolute vorticity from an arbitrarily selected thunderstorm, the WRF model successfully captures the supercellular convection and the corresponding mesocyclone structure. Accordingly, short-term weather forecasts and severe weather warnings might greatly benefit from such high-resolution WRF simulations. The extensive low-reflectivity (20–30 dBZ) area accompanying the convective cells is better captured by the Thompson microphysical parameterization than the Morrison scheme. Therefore, it is suggested that the complexity and thus higher computational demand of a full two-moment microphysical parameterization do not necessarily improve model performance, which is important from an operative numerical weather prediction perspective.

In the future, WRF simulations with finer grid spacing (at the order of 100 m) could be carried out to successfully capture the storm merger process and the fine-scale details of the tornado-producing supercell. An extensive analysis of the physical-dynamical settings of the model is also recommended.

Acknowledgement: The authors are grateful to the Hungarian Meteorological Service (OMSZ) and the Slovak Hydrometeorological Institute for making the data available for research. The research leading to this paper was supported by the Hungarian Scientific Research Fund under the grant FK132014. Hajnalka Breuer's work was additionally financed by the János Bolyai Research Scholarship of the Hungarian Academy of Sciences.

References

- Beck, J. and C. Weiss, 2013: An assessment of low-level baroclinity and vorticity within a simulated supercell. *Month. Weather Rev.* 141, 649–669. <https://doi.org/10.1175/MWR-D-11-00115.1>
- Benjamin, S.G., Weygandt, S.S., Brown, J.M., Hu, M., Alexander, C.R., Smirnova, T.G., Olson, J.B., James, E.P., Dowell, D.C., Grell, G.A., and Lin, H., 2016: A North American hourly assimilation and model forecast cycle: The Rapid Refresh. *Month. Weather Rev.* 144, 1669–1694. <https://doi.org/10.1175/MWR-D-15-0242.1>
- Betten, D.P., Biggerstaff, M.I., and Ziegler, C.L., 2018: Three-Dimensional Storm Structure and Low-Level Boundaries at Different Stages of Cyclic Mesocyclone Evolution in a High-Precipitation Tornadic Supercell. *Adv. Meteorol.* 2018, 1–24. <https://doi.org/10.1155/2018/9432670>
- Bluestein, H.B. and M. L. Weisman, 2000: The interaction of numerically simulated supercells initiated along lines. *Month. Weather Rev.* 128, 3128–3149. [https://doi.org/10.1175/1520-0493\(2000\)128%3C3128:TIONSS%3E2.0.CO;2](https://doi.org/10.1175/1520-0493(2000)128%3C3128:TIONSS%3E2.0.CO;2)
- Bunkers, J.M., Klimowski, B.A., Zeitler, J.W., Thompson, R.L., and Weisman, M.L., 2000: Predicting Supercell Motion Using a New Hodograph Technique. *Weather and Forecast.* 15, 61–79. [https://doi.org/10.1175/1520-0434\(2000\)015%3C0061:PSMUAN%3E2.0.CO;2](https://doi.org/10.1175/1520-0434(2000)015%3C0061:PSMUAN%3E2.0.CO;2)

- Dawson, D.T., Xue, M., Milbrandt, J.A., and Yau, M.K., 2010: Comparison of evaporation and cold pool development between single-moment and multimoment bulk microphysics schemes in idealized simulations of tornadic thunderstorms. *Month. Weather Rev.* 138, 1152–1171. <https://doi.org/10.1175/2009MWR2956.1>
- Gordon, J.D. and Albert D., 2000: A Comprehensive Severe Weather Forecast Checklist and Reference Guide. US Department of Commerce, National Oceanic and Atmospheric Administration, National Weather Service, Scientific Services Division, Central Region: Missouri.
- Hastings, R. and Richardson, Y., 2016: Long-Term Morphological Changes in Simulated Supercells Following Mergers with Nascent Supercells in Directionally Varying Shear. *Month. Weather Rev.* 144, 471–499. <https://doi.org/10.1175/MWR-D-15-0193.1>
- Hong, S.-Y., Noh, Y., and Dudhia, J., 2006: A new vertical diffusion package with an explicit treatment of entrainment processes. *Month. Weather Rev.* 134, 2318–2341. <https://doi.org/10.1175/MWR3199.1>
- Iacono, M.J., Delamere, J.S., Mlawer, E.J., Shephard, M.W., Clough, S.A., and Collins, W.D., 2008: Radiative forcing by long-lived greenhouse gases: Calculations with the AER radiative transfer models. *J. Geophys. Res-Atmos.* 113(D13). <https://doi.org/10.1029/2008JD009944>
- Jaret, W., Rogers, A., and Weiss, C.C., 2008: The association of cell mergers with tornado occurrence. Poster Presentation 24th Conference on Severe Local Storms. Savannah, Georgia.
- Jiménez, P.A., Dudhia, J., González-Rouco, J.F., Navarro, J., Montávez, J.P., and García-Bustamante, E., 2012: A revised scheme for the WRF surface layer formulation. *Month. Weather Rev.* 140, 898–918. <https://doi.org/10.1175/MWR-D-11-00056.1>
- Johnson, M., Jung, Y., Dawson, D.T., and Xue, M., 2016: Comparison of simulated polarimetric signatures in idealized supercell storms using two-moment bulk microphysics schemes in WRF. *Month. Weather Rev.* 144, 971–996. <https://doi.org/10.1175/MWR-D-15-0233.1>
- Jung, Y., Xue, M., and Tong, M., 2012: Ensemble Kalman filter analyses of the 29–30 May 2004 Oklahoma tornadic thunderstorm using one-and two-moment bulk microphysics schemes, with verification against polarimetric radar data. *Month. Weather Rev.* 140, 1457–1475. <https://doi.org/10.1175/MWR-D-11-00032.1>
- Knupp, K.R., Murphy, T.A., Coleman, T.A., Wade, R.A., Mullins, S.A., Schultz, C.J., Schultz, E.V., Carey, L., Sherrer, A., McCaul Jr., E.W., Carcione, B., Latimer, S., Kula, A., Laws, K., Marsh, P.T., and Klockow, T., 2014: Meteorological Overview of the Devastating 27 April 2011 Tornado Outbreak. *Bull. Amer. Meteorol. Soc.* 95, 1041–1062. <https://doi.org/10.1175/BAMS-D-11-00229.1>
- Lee, B.D., Jewett, F., and Wilhelmson, R. B., 2006: The 19 April 1996 Illinois tornado outbreak. Part II: Cell Mergers and associated tornado incidence, *Weather Forecast.* 21, 449–446. <https://doi.org/10.1175/WAF943.1>
- Markowski, P., Rasmussen, E.N., and Straka, J.M., 1998: The Occurrence of Tornadoes in Supercells Interacting with Boundaries during VORTEX-95. *Weather Forecast* 13, 852–859. [https://doi.org/10.1175/1520-0434\(1998\)013%3C0852:TOOTIS%3E2.0.CO;2](https://doi.org/10.1175/1520-0434(1998)013%3C0852:TOOTIS%3E2.0.CO;2)
- Marquis, J., Richardson, Y., Wurman, J., and Markowski, P., 2008: “Single- and dual-Doppler analysis of a tornadic vortex and surrounding storm-scale flow in the Crowell, Texas, supercell of 30 April 2000,” *Month. Weather Rev.* 136, 5017–5043. <https://doi.org/10.1175/2008MWR2442.1>
- Miglietta, M.M., Mazon, J., and Rotunno, R., 2017: Numerical simulations of a tornadic supercell over the Mediterranean. *Weather Forecast.* 32, 1209–1226. <https://doi.org/10.1175/WAF-D-16-0223.1>
- Morrison, H., Thompson, G., and Tatarskii, V., 2009: Impact of Cloud Microphysics on the Development of Trailing Stratiform Precipitation in a Simulated Squall Line: Comparison of One- and Two-Moment Schemes. *Month. Weather Rev.* 137, 991–1007. <https://doi.org/10.1175/2008MWR2556.1>
- Niu, G.Y., Yang, Z.L., Mitchell, K.E., Chen, F., Ek, M.B., Barlage, M., Kumar, A., Manning, K., Niyogi, D., Rosero, E., and Tewari, M., 2011: The community Noah land surface model with multiparameterization options (Noah-MP): 1. Model description and evaluation with local-scale measurements. *J. Geophys. Res-Atmos.* 116(D12). <https://doi.org/10.1029/2010JD015139>
- Orf, L., Wilhelmson, R., Lee, B., Finley, C., Houston, A., 2017: Evolution of a Long-Track Violent Tornado within a Simulated Supercell. *Bull. Amer. Meteorol. Soc.* 98, 45–68. <https://doi.org/10.1175/BAMS-D-15-00073.1>

- Pilguy, N., Taszarek, M., Pajurek, E., and Kryza, M., 2019: High-resolution simulation of an isolated tornadic supercell in Poland on 20 June 2016. *Atmosph. Res.* 218, 145–159. <https://doi.org/10.1016/j.atmosres.2018.11.017>
- Powers, J.G., Klemp, J.B., Skamarock, W.C., Davis, C.A., Dudhia, J., Gill, D.O., Coen, J.L., Gochis, D.J., Ahmadov, R., Peckham, S.E., and Grell, G.A., 2017: The weather research and forecasting model: Overview, system efforts, and future directions. *Bull. Amer. Meteorol. Soc.* 98, 1717–1737. <https://doi.org/10.1175/BAMS-D-15-00308.1>
- Scheffknecht, P., Serafin, S., and Grubišić, V., 2017: A long-lived supercell over mountainous terrain. *Quart. J. Roy. Meteorol. Soc.* 143(709), 2973–2986. <https://doi.org/10.1002/qj.3127>
- Schueth, A., Weiss, C., and Dahl, J.M.L., 2021: Comparing Observations and Simulations of the Streamwise Vorticity Current and the Forward-Flank Convergence Boundary in a Supercell Storm. *Month. Weather Rev.* 149, 1651–1671. <https://doi.org/10.1175/MWR-D-20-0251.1>
- Simpson, J., Westcott, N.E., Clerman, R.J., and Peilke, R.A., 1980: On cumulus mergers. *Archiv für Meteorologie, Geophysik Bioklimatol. Ser. A*, 29, 1–40. <https://doi.org/10.1007/BF02247731>
- Skamarock, W.C., Klemp, J.B., Dudhia, J., Gill, D.O., Liu, Z., Berner, J., Wang, W., Powers, J.G., Duda, M.G., Barker, D.M., and Huang, X-Y., 2019: A Description of the Advanced Research WRF Model Version 4. NCAR Tech Note NCAR/TN-556+STR, Mesoscale and Microscale Meteorology Division, Boulder CO, USA. <https://doi.org/10.5065/1dfh-6p97>
- Spiridonov, V., Čurić, M., Velinov, G., and Jakimovski, B., 2021: Numerical simulation of a violent supercell tornado over Vienna airport initialized and initiated with a cloud model. *Atmosph. Res.* 261, 105758. <https://doi.org/10.1016/j.atmosres.2021.105758>
- Thompson, G., Field, P.R., Rasmussen, R.M., and Hall, W.D., 2008: Explicit forecasts of winter precipitation using an improved bulk microphysics scheme. Part II: Implementation of a new snow parameterization. *Month. Weather Rev.* 136, 5095–5115. <https://doi.org/10.1175/2008MWR2387.1>
- Van Leer, K.W., 2013: Storm mergers and their role in tornado genesis during the 2011 Joplin storm. *Graduate Thesis*, 1–77., Department of Atmospheric Sciences, University of Illinois Urbana-Champaign, Illinois. <http://hdl.handle.net/2142/44134>
- Westcott, N. and Kennedy, P.C., 1989: Cell development and merger in an Illinois thunderstorm observed by Doppl radar. *J. Atmosph. Sci.* 46, 117–131. [https://doi.org/10.1175/1520-0469\(1989\)046%3C0117:CDAMIA%3E2.0.CO;2](https://doi.org/10.1175/1520-0469(1989)046%3C0117:CDAMIA%3E2.0.CO;2)
- Westcott, N., 1994: Merging of convective clouds: Cloud initiation, bridging, and subsequent growth. *Month. Weather Rev.* 122, 780–790. [https://doi.org/10.1175/1520-0493\(1994\)122%3C0780:MOCCCI%3E2.0.CO;2](https://doi.org/10.1175/1520-0493(1994)122%3C0780:MOCCCI%3E2.0.CO;2)
- Wood, V.T., Brown, R.A., and Dowell, D.C., 2009: Simulated WSR-88D Velocity and Reflectivity Signatures of Numerically Modeled Tornadoes. *J. Atmosph. Ocean. Technol.* 26, 876–893. <https://doi.org/10.1175/2008JTECHA1181.1>
- Wurman, J., Y. Richardson, C. Alexander, S. Weygandt, and P.F. Zhang, 2007: Dual-Doppler and Single-Doppler Analysis of a Tornadic Storm Undergoing Mergers and Repeated Tornadogenesis. *Month. Weather Rev.* 135, 736–758. <https://doi.org/10.1175/MWR3276.1>